Journal of Microbiological Methods 166 (2019) 105716

Contents lists available at ScienceDirect

Journal of Microbiological Methods

journal homepage: www.elsevier.com/locate/jmicmeth

Myristica fragrans bio-active ester functionalized ZnO nanoparticles exhibit antibacterial and antibiofilm activities in clinical isolates

Tijo Cherian[a], Khursheed Ali[a], Saher Fatima[a], Quaiser Saquib[b], Sabiha M. Ansari[c], Hend A. Alwathnani[c], Abdulaziz A. Al-Khedhairy[b], Majed Al-Shaeri[d], Javed Musarrat[a,e,*]

[a] Faculty of Agricultural Sciences, Department of Agricultural Microbiology, Aligarh Muslim University, Aligarh-202002, Uttar Pradesh, India.
[b] Zoology Department, College of Sciences, King Saud University, P.O. Box 2455, Riyadh 11451, Saudi Arabia.
[c] Department of Botany & Microbiology, College of Sciences, King Saud University, P.O. Box 2455, Riyadh 11451, Saudi Arabia.
[d] Faculty of Science, Department of Biological Sciences, King Abdulaziz University, Jeddah, Saudi Arabia.
[e] School of Biosciences and Biotechnology, Baba Ghulam Shah Badshah University, Rajouri, Jammu & Kashmir, India.

ARTICLE INFO

Keywords:
M. fragrans bio-actives
Esters capped-ZnO
Antibiofilm
GC–MS

ABSTRACT

We provide a novel one-step/one-pot bio-inspired method of synthesis for *Myristica fragrans* leaf ester (MFLE) capped-zinc oxide nanoparticles (MFLE-ZnONPs). Antibacterial and antbiofilm efficacies of MFLE-ZnONPs were tested against the multi-drug resistant (MDR) *Escherichia coli* (*E. coli*-336), methicillin-resistant *Staphylococcus aureus* (MRSA-1) and methicillin-sensitive (MSSA-2) clinical isolates. Antibacterial screening using well diffusion assay revealed the cytotoxicity of MFLE-ZnONPs in the range of 500-2000 μg/ml. MFLE-ZnONPs significantly increased the zone of growth inhibition of *E. coli*-336 (17.0 ± 0.5 to 19.25 ± 1.0 mm), MSSA-2 (16.75 ± 0.8 to 19.0 ± 0.7 mm) and MRSA-1 (16.25 ± 1.0 to 18.25 ± 0.5 mm), respectively. The minimum inhibitory concentration (MIC) and minimum bactericidal concentrations (MBC) against *E. coli*-336, MRSA-1 and MSSA-2 were found to be 1500, 1000 and 500 μg/ml, and 2500, 2000 and 1500 μg/ml, respectively. A time and dose dependent reduction in the cell proliferation were also found at the respective MICs of tested strains. Scanning electron microscopy (SEM) of MFLE-ZnONPs-treated strains exhibited cellular damage *via* loss of native rod and coccoid shapes because of the formation of pits and cavities. *E. coli*-336 and MRSA-1 strains at their MICs (1500 and 1000 μg/ml) sharply reduced the biofilm production to 51% and 24%. The physico-chemical characterization *via* x-ray diffraction (XRD) ascertained the crystallinity and an average size of MFLE-ZnONPs as 48.32 ± 2.5 nm. Gas chromatography-mass spectroscopy (GC–MS) analysis of MFLE-ZnONPs unravelled the involvement of two bio-active esters (1) butyl 3-oxobut-2-yl ester and (2) α-monoolein) as surface capping/stabilizing agents. Fourier transform infrared (FTIR) analysis of MFLE and MFLE-ZnONPs showed the association of amines, alkanes, aldehydes, amides, carbonyl and amines functional groups in the corona formation. Overall, our data provide novel insights on the rapid development of eco-friendly, cost-effective bio-synthesis of MFLE-ZnONPs, showing their putative application as nano-antibiotics against MDR clinical isolates.

1. Introduction

Zinc oxide (ZnO) has a wide spectrum of applications owing to its intrinsic physico-chemical properties including large band gap (3.33 eV) and exciton energy (60 meV). Such unique characteristics have extended the entry of ZnO into next generation optoelectronics (Look et al., 1998; Tang et al., 1998) as well as application in ultra-violet (UV) lasers and light-emitting diodes (Aoki and Hatanaka, 2000; Pearton et al., 2004). Nanoscale metal and metal oxide particles possess tremendously large surface area and active sites allowing them to function as efficient catalysts (Shahbazali et al., 2014; Bhosale and Bhanage, 2015). Nano-sized ZnO structures also provide a strong foundation for their use in biomedical settings and the agriculture sector (Sangani et al., 2015; Hameed et al., 2016), amounting to global consumption of 10^5 tons per year (Das et al., 2011). Furthermore, incorporation of ZnONPs into periodontal membranes can be used as a barrier for evading the colonization of *Porphyromonas gingivalis,* which is commonly involved in inducing periodontitis (Nasajpour et al., 2017).

Nanotechnologists have explored a diverse set of plant-based bio-inspired methods of NPs fabrication (Musarrat et al., 2015; Ali et al., 2015; Ali et al., 2016; Ali et al., 2018; Ali et al., 2019). During the last two decades, indigenous bio-actives present in the root, leaf and fruit

* Corresponding author at: Department of Agricultural Microbiology, Faculty of Agricultural Sciences, Aligarh Muslim University, Aligarh-202002, Uttar Pradesh, India.
E-mail address: musarratj1@yahoo.com (J. Musarrat).

https://doi.org/10.1016/j.mimet.2019.105716
Received 16 June 2019; Received in revised form 4 September 2019; Accepted 5 September 2019
Available online 06 September 2019

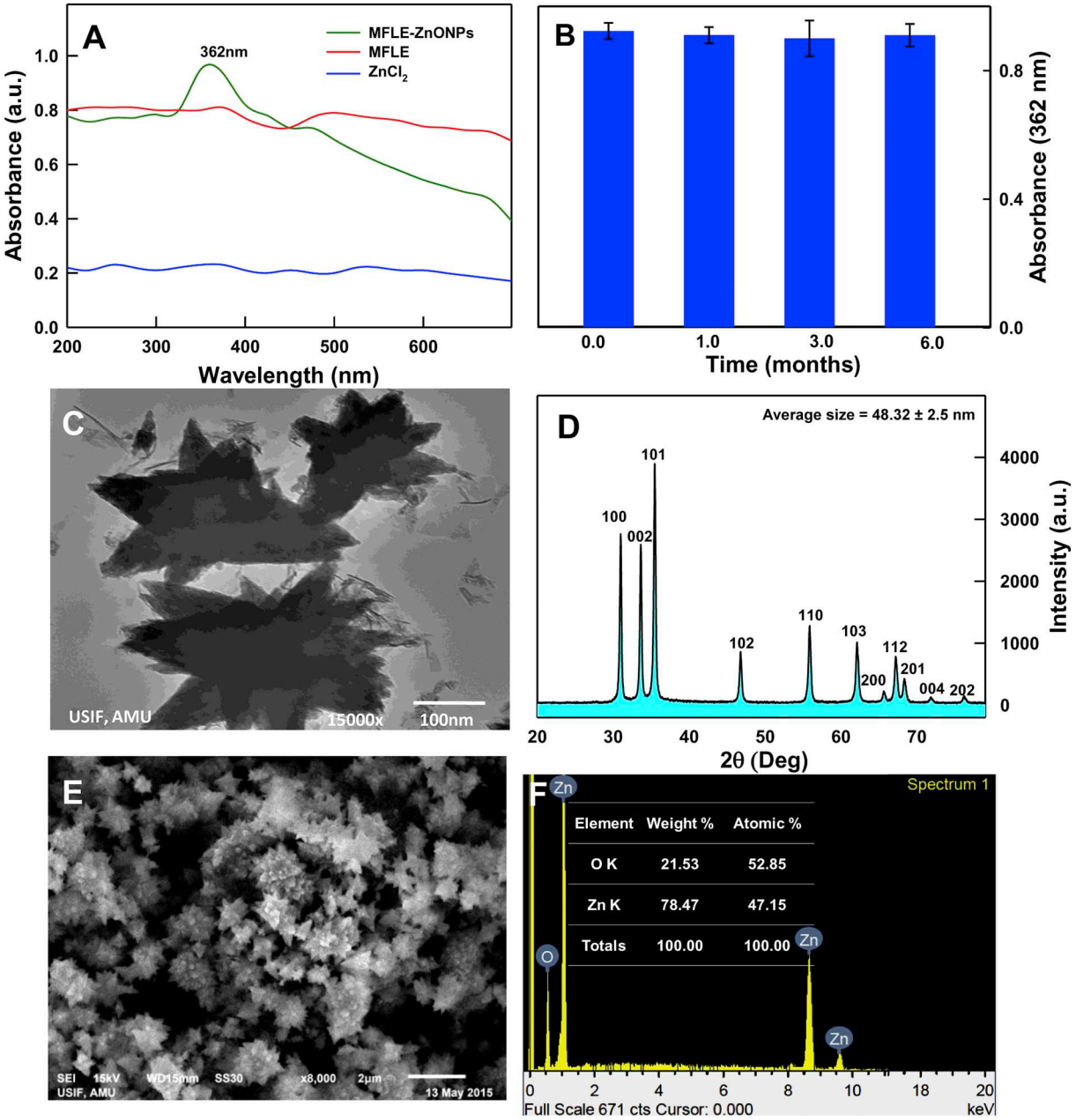

Fig. 1. Physico-chemical characterization of MFLE-ZnONPs. Panel A represents UV–Vis spectra of MFLE, $ZnCl_2$ and MFLE-ZnONPs showing a sharp peak of MFLE-ZnONPs appeared due to SPR at λ_{max} 362 nm. Panel B shows stability of MFLE-ZnONPs based on SPR measurements up to six months (error bars represent the mean ± SE of three replicates). Panel C shows a representative TEM image of flower shaped MFLE-ZnONPs. Panel D demonstrates X-ray diffraction patterns of biologically synthesized MFLE-ZnONPs. Panel E represents SEM image showing nano sized flower MFLE-ZnO, whereas Panel F represents the energy dispersive X-ray spectrum of MFLE–ZnONPs.

extracts of plants have exhibited their innate ability to reduce a wide range of metal ions to nanoparticles (NPs) (Musarrat et al., 2015; Ali et al., 2015; Ali et al., 2016; Ali et al., 2018; Ali et al., 2019). Bio-synthesis of metallic NPs using plant extracts has gained significant attraction due to their procedural comprehensiveness, cost-effectiveness and eco-friendliness, as compared to the chemical method, which is complicated, expensive and hazardous in nature. In fact, the green approach of bio-inspired fabrication of NPs can be performed in-house without involvement of any expensive and high energy consuming equipment, and specific experimental conditions. A wide variety of metal based nanostructures have been synthesiszed *via* one-pot bio-inspired/biofabrication approach by using *Eucalyptus globulus* (Ali et al., 2016), bell paper (Ahmed et al., 2018), *Nepeta deflersiana* (Al-Sheddi et al., 2018), and *Aloe vera* (Ali et al., 2016; Ali et al., 2018) extracts as reducing and capping agents for silver (Ag), zinc oxide (ZnO) and hematite (α-Fe_2O_3) NPs.

Myristica fragrans popularly known as nutmeg is an evergreen, tall plant belonging to the family "*Myristicaceae*". Flavonols, flavones, flavanones, chalcones, isoflavonoids, and anthocyanins have been reported in crude extract and essential oil of *M. fragrans* which may have antimicrobial, antioxidant and anticancer activities (Helen et al., 2012; Lima et al., 2012). The bio-actives reported in MFLE have been identified in various plant extracts showing the potential of bio-fabricating a wide range of metal ions into nanostructures (Musarrat et al., 2015; Ali et al., 2015; Ali et al., 2016; Ali et al., 2018; Ali et al., 2019; Ahmed et al., 2018). Besides, *M. fragrans* seed essential oil bio-actives *viz.* eugenol, isoelemicin, isoeugenol, methoxy eugenol, myristic acid, and myristicin have been employed as organic-templates/scaffolds in order to fabricate

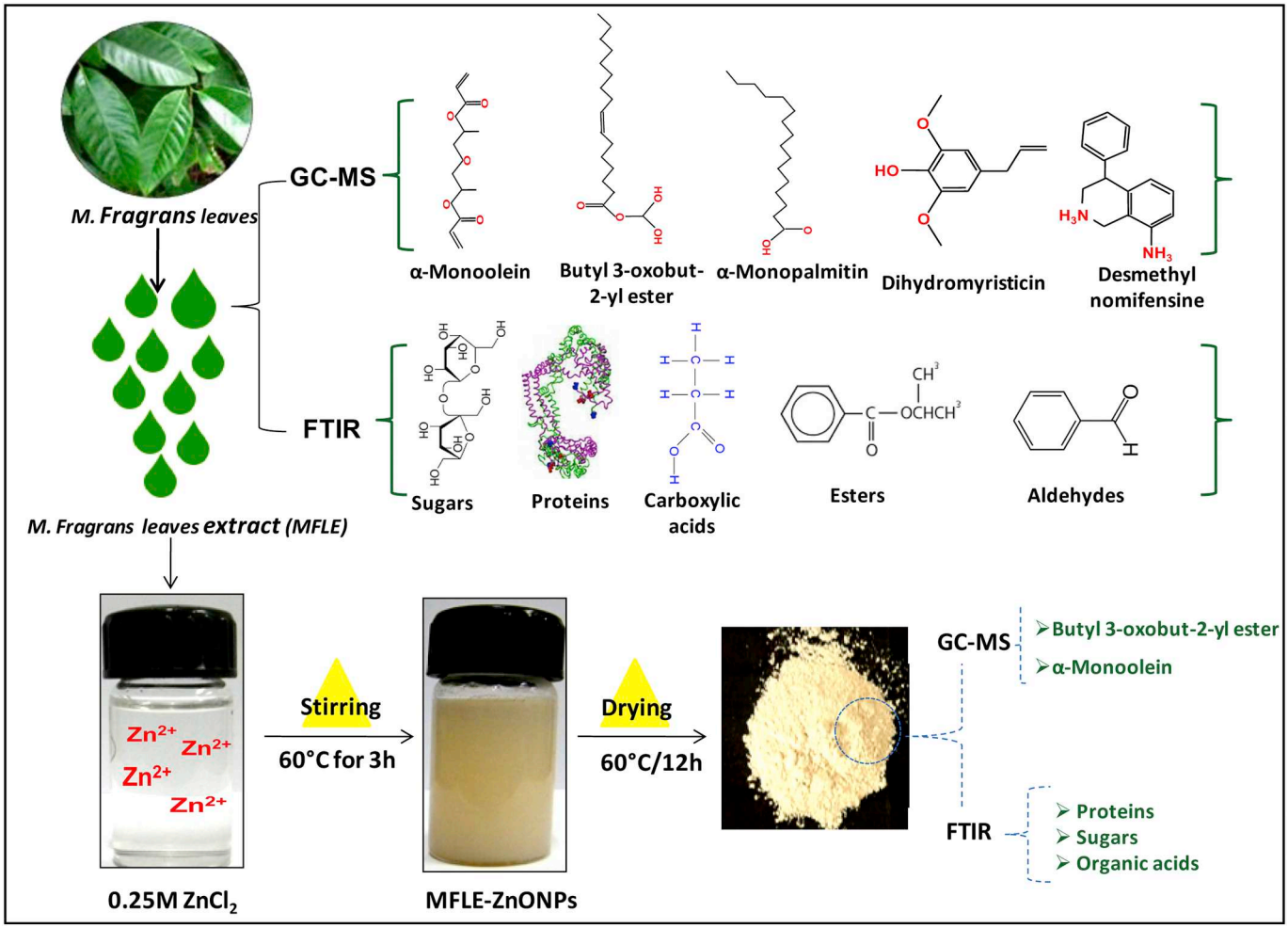

Fig. 2. Schematic representation of MFLE-ZnONPs formation.

Ag^{+} into AgNPs biologically against MDR *Salmonella enterica* (Balakrishnan et al., 2017), *E. coli* and *S. aureus* (Sharma et al., 2014). *M. fragrans* leaves containing aromatic essential oil admixtured in acetone has also been implicated to synthesize ZnONPs showing its cytotoxic effects in liver cancer cells (HepG2) (Ashokan et al., 2017). Recently, Nasajpour et al. (2018) have demonstrated that the encapsulation of different-shape particles significantly influences the physicochemical and biological activities of such resultant composite scaffolds. Taken together, the bio-actives of MFLE and wide spectrum of applications of ZnONPs has led us to investigate the crude aqueous extract of MFLE as a reducing, capping and stabilizing agent for the bio-synthesis of MFLE capped ZnONPs (MFLE-ZnONPs). To the best of our knowledge, there is no such comprehensive and systematic report demonstrating precisely two bio-active esters of MFLE namely (1) butyl 3-oxobut-2-yl ester ($C_{12}H_{18}O_5$) and (2) α-monoolein ($C_{21}H_{40}O_4$) that reduce Zn^{2+} to ZnONPs. The present work is the first report on MFLE-ZnONPs as potential antibacterial and antibiofilm agents against MDR clinical isolates. Hence, this study was aimed to (i) synthesize the ZnONPs using MFLE extracts (ii) characterization of biogenically synthesiszed MFLE-ZnONPs (iii) analysis of bio-active compounds of MFLE-ZnONPs, (iv) antibacterial and antibiofilm potential of MFLE-ZnONPs against clinical isolates.

2. Materials and methods

2.1. Bacterial strains

Gram-positive methicillin-resistant *S. aureus*-1 (MRSA-1), Gram-positive methicillin-sensitive *S. aureus*-2 (MSSA-2) and Gram-negative extended spectrum β-lactamase (ESβL) producing *E. coli*-336 (*E. coli*-336) isolates were obtained from Department of Microbiology, Jawaharlal Nehru Medical College and Hospital, Aligarh Muslim University, India. The bacterial isolates were cultured aseptically in Luria-Bertani (LB) medium (Hi-media, Pvt. Ltd. Mumbai, India) at 37 °C/180 rpm overnight and preserved at −20 °C in 20% glycerol.

2.2. M. fragrans leaf extract (MFLE) preparation

Green leaves of *M. fragrans* were collected from forest cover range at Kottayam district (9.4710933°N, 76.765°E) Kerala, India and verified by taxonomist, Department of Botany, Aligarh Muslim University, India. *M. fragrans* leaves (50 g) were thoroughly washed with double distilled water and ground to a green paste by using a domestic mixer grinder (Prestige Pvt. Ltd. India). Autoclaved Milli Q water (100 ml) was added to the paste and kept for 20 min at room temperature. Aqueous *M. fragrans* leaves extract (MFLE) was then filtered through Whatman paper No.1 filter paper and stored at 4 °C until used.

2.3. Synthesis of MFLE-ZnONPs

Bio-inspired synthesis of *M. fragrans*-capped-ZnONPs (MFLE-ZnONPs) was carried out by modifying our previously described method (Ali et al., 2016). In brief, MFLE (10 ml) was added to 90 ml of aqueous zinc chloride ($ZnCl_2$) solution maintaining its 0.25 M concentration in the final volume (100 ml) of MFLE-$ZnCl_2$ reaction mixture (1:9 *v*/v). MFLE-$ZnCl_2$ mixture was stirred for 3 h at 60 °C. The transparent reaction mixture turned to pale yellow precipitate at pH 12.0

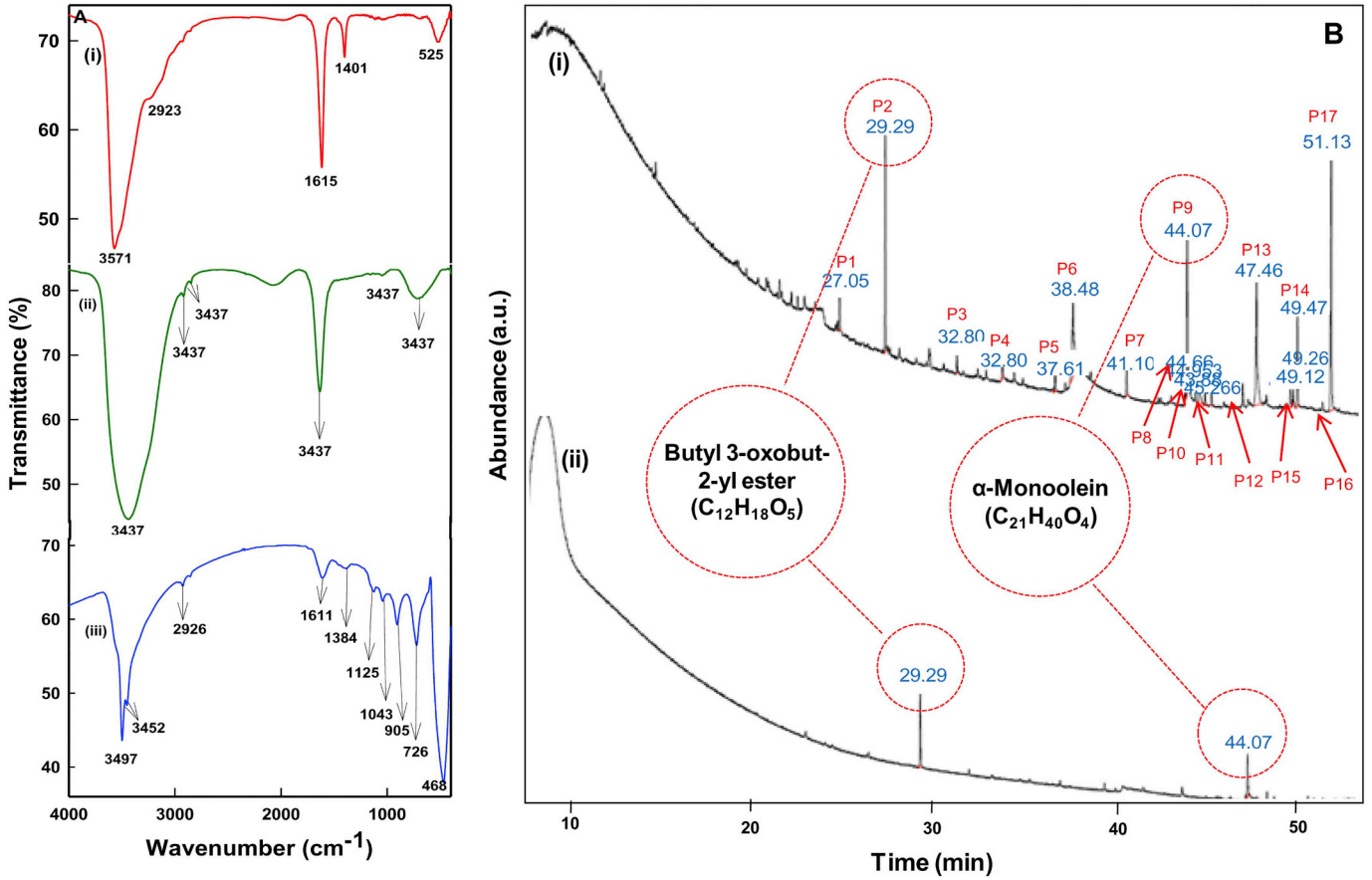

Fig. 3. FTIR and GC–MS analyses. (A) FTIR spectral analyses of pristine $ZnCl_2$ solution (spectrum-i), *M. fragrance* leaf extract alone (spectrum-ii) and MFLE-ZnONPs (spectrum-iii). (B) GC–MS analysis (spectrum-i) shows typical chromatogram of MFLE indicating 17 peaks for 15 different bio-actives, whereas spectrum-ii shows two MFLE compounds: butyl 3-oxobut-2-yl ester and α-monoolein, associated with ZnONPs.

when 1 M NaOH was added. Precipitate was pelleted, washed, dried, processed for physico-chemical characterization as described earlier (Ali et al., 2016).

2.4. Characterization of MFLE-ZnONPs

The characterization of MFLE-ZnONPs was achieved by following our previously described method (Ali et al., 2016). The surface plasmon resonance (SPR) peak of ZnONPs was acquired through a double beam UV–Vis spectrophotometer (UV5704S, Electronics, India Ltd). The crystallinity and average size were determined by X-ray diffraction (XRD) (Rigaku Corporation, Tokyo, Japan). Morphological and elemental compositions were analyzed on scanning electron (SEM-EDX) and transmission electron microscopy (TEM) (JEOL, Tokyo, Japan).

2.5. FTIR and GC–MS analyses of MFLE-ZnONPs

For FTIR, MFLE (alone) and MFLE-ZnONPs were mixed with spectroscopic grade KBr in 1:100 ratio separately and the spectra were recorded on Perkin Elmer FTIR spectrometer, Spectrum Two (CT, USA) (Ali et al., 2018). MFLE and MFLE-ZnONPs in a volume of 5 ml were analyzed for GC–MS following the previously described instrument parameters (Ali et al., 2018).

2.6. Antibacterial studies

2.6.1. Well diffusion assay

The overnight grown cultures of *E. coli*-336 and MRSA-1and MSSA-2 (OD_{600} = 0.1 ≅10^7 colony forming unit (CFU)/ml) were evenly spread on Luria-Bertani agar (LBA) plates. MFLE-ZnONPs (500, 1000, 1500 and 2000 μg/ml) in a volume of 100 μl were dispensed in precut wells, sealed with 0.7% agar. Aqueous MFLE (10%) was used as control. All plates were incubated for 24 h at 37 °C followed by analysis of growth inhibition (Ali et al., 2015).

2.6.2. MIC and MBC determination

For the minimum inhibitory concentration (MIC) and minimum bactericidal concentrations (MBC), the overnight grown cultures of *E. coli*-336, MRSA-1 and MSSA-2 were diluted to OD_{600} = 0.1 (≅10^7CFU/ml) in LB medium and incubated with 125, 250, 500, 1000 and 2000 μg/ml of MFLE-ZnONPs for 24 h at 37 °C followed by effect analysis (Ali et al., 2015).

2.6.3. Comparative assessment of bacterial growth inhibition

Overnight grown cultures of *E. coli*-336, MRSA-1 and MSSA-2 (100 μl) were separately added to 5 ml of LB supplemented with MFLE (10% *v*/v), $ZnCl_2$ (0.25 M) and MIC (1500 μg/ml) of MFLE-ZnONPs. Untreated bacterial isolates were used as control. Changes in the bacterial growth were read at OD_{600nm} as described previously (Ali et al., 2016).

2.6.4. Bacterial interaction with MFLE-ZnONPs

E. coli-336 and MRSA-1 were treated with 250 μg/ml of MFLE-ZnONPs for 24 h at 37 °C. Cells were pelleted at 3000 rpm for 5 min and fixed for 4 h with glutaraldehyde (2.5%). Cells were dehydrated with ascending grade of ethanol for the structural analysis on SEM as described earlier (Ali et al., 2018).

Table 1
GC–MS analysis of *M. fragrans* leaf extract.

S.No. of peaks (P)	Retention time (R_T)	Name of compound	Mol. Wt.	Mol. formula	Peak area (%)	Structure
1	27.056	4-Methoxysafrole	192.21	$C_{11}H_{12}O_3$	2.278	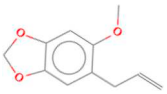
2	29.295	Butyl 3-oxobut-2-yl ester	242.26	$C_{12}H_{18}O_5$	13.531	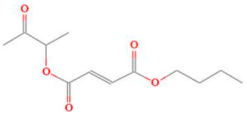
3	32.802	5-Amino-1-methyl-, ethyl ester	169.18	$C_7H_{11}N_3O_2$	1.125	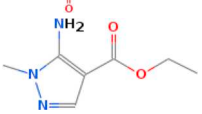
4	35.032	n-Hexadecanoic acid	256.42	$C_{16}H_{32}O_2$	1.244	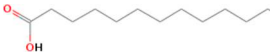
5	37.611	α,γ-Dipalmitin	296.48	$C_{19}H_{36}O_2$	1.523	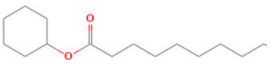
6	38.485	Cis-13-Octadecenoic acid	282.46	$C_{18}H_{34}O_2$	13.865	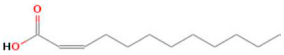
7	41.108	1-Palmityl-2-acetyl-3-myristoyl-sn-glycerol	568.91	$C_{35}H_{68}O_5$	1.996	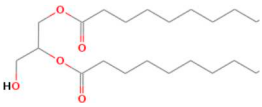
8	43.981	Butyl linoleate	336.55	$C_{22}H_{40}O_2$	0.968	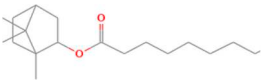
9	44.079	α-Monoolein	356.53	$C_{21}H_{40}O_4$	10.71	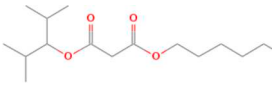
10	44.668	α-Monopalmitin	330.5	$C_{19}H_{38}O_4$	3.265	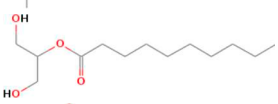
11	44.953	Isooctyl phthalate	390.55	$C_{24}H_{38}O_4$	1.036	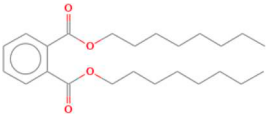
12	45.266	9-Hydroxytridecyl docosanoate	538.92	$C_{35}H_{70}O_3$	0.84	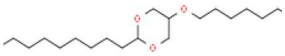
13	47.469	α-Monoolein	356.53	$C_{21}H_{40}O_4$	16.052	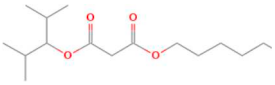
14	49.129	Coniferic acid	194.18	$C_{10}H_{10}O_4$	1.563	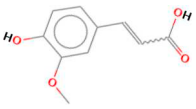
15	49.263	Dihydromyristicin	194.22	$C_{11}H_{14}O_3$	0.869	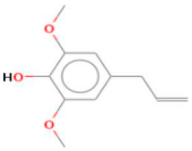
16	49.477	Dihydromyristicin	194.22	$C_{11}H_{14}O_3$	6.12	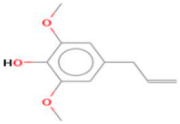
17	51.136	Desmethyl nomifensine	224.3	$C_{15}H_{16}N_2$	22.989	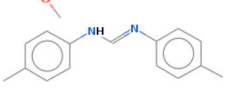

2.6.5. Effect on biofilm formation

Quantitative estimation of biofilm inhibiton was done using (100 µl) of overnight grown test isolates (≅10^7 CFU/ml), treated separately with 250-2000 µg/ml of MFLE-ZnONPs for 24 h. The treated cells were then seeded in 96-well plates, incubated, stained and absorbance was taken at OD_{490nm} as described previously (Ali et al., 2016).

For the qualitative analysis of biofilm formation, bacterial isolates were exposed to above concentrations of MFLE-ZnONPs, and allowed to grow on sterile glass coverslips for 24 h at 37 °C. Coverslips were then subjected to washing, staining and microscopic observations for biofilm disruption following previously described method (Ali et al., 2018).

Table 2
GC–MS analysis of *M. fragrans* capped ZnONPs.

S.No. of ppeaks (P).	Retention time (R_T)	Name of compound	Mol. Wt.	Mol. formula	Peak area (%)	Structure
1	29.295	Butyl 3-oxobut-2-yl ester	242.26	$C_{12}H_{18}O_5$	13.531	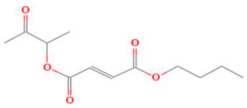
2	44.079	α-Monoolein	356.53	$C_{21}H_{40}O_4$	16.052	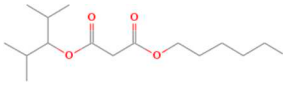

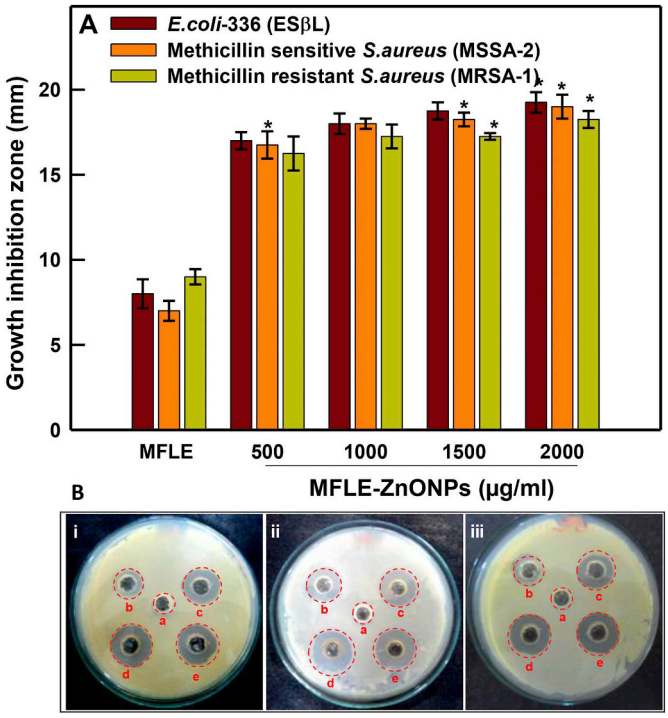

Fig. 4. Evaluation of Antibacterial activity. (A) Assessment of antibacterial activity of MFLE alone and MFLE-ZnONPs by well diffusion assay. A volume of 100 µl MFLE (10%) was taken as control. Each histogram represents the mean ± SD of two independent experiments done in triplicate. (B) Representative culture plates of (i) Gram-negative (ESβL producing) *E. coli*-336 (ii) Gram-positive (methicillin-resistant) *S. aureus* (MRSA-1) (iii) and (methicillin-sensitive) *S. aureus* (MSSA-2) exhibiting zone of growth inhibition at (a) 10% MFLE and, (b) 500, (c) 1000, (d) 1500 and, (e) 2000 µg/ml of MFLE-ZnONPs after 24 h.

Table 3
Assessment of MIC and MBC of MFLE-ZnONPs against clinical isolates.

MFLE-ZnONPs (µg/ml)		
Bacterial strain	MIC	MBC
E.coli-336	1500	2500
MRSA-1	1000	2000
MSSA-2	500	1500

2.7. Statistics

The statistical analyses of data were done on Sigma Plot 11.0 (Sigma Plot 11.0, Inc., USA). A Holm-Sidak test for multiple comparisons *versus* a control group was used for one-way analysis of variance (ANOVA). The data were expressed as mean ± SD of at least three independent experiments done in triplicate. The differences were considered statistically significant if $*p < 0.05$ unless otherwise stated.

3. Results and discussion

3.1. Bio-synthesis and UV–Vis analysis of MFLE-ZnONPs

UV–Vis data of MFLE-ZnONPs exhibited a characteristic absorption peak at 362 nm, while MFLE and $ZnCl_2$ alone showed no peaks at the same wavelength (Fig. 1A). Similar UV–Vis absorption bands have also been reported in the range of 358–375 nm in *Aloe vera* mediated bio-synthesis of ZnONPs (Sangeetha et al., 2011; Ali et al., 2016). The UV–Vis spectrophotometric analysis of colloidal reaction mixture showed peaks at 362 nm for a period of 6 months, hence, verifying the stability of MFLE-ZnONPs with no precipitation (Fig. 1B). The MFLE bio-actives primarily comprised of myristicin, sabinene, β-pinene, α-pinene, iso-eugenol, p-cymene, carvacrol, eugenol and β-caryophellene endowed with intrinsic ability to reduce metal ions, for example, Fe^{3+} to Fe^{2+} (Gupta et al., 2013) and Ag^{+} to Ag^{0} (Vilas et al., 2014), serving as a stable electron donor. Hence, it is speculated that the MFLE bio-actives have played a significant role in reducing Zn^{2+} into ZnO^{0} NPs (Sutradhar and Saha, 2015), as also evident with a simultaneous change in the transparent reaction mixture to pale white precipitate (Fig. 2). Similar color change has also been recorded in earlier studies due to excitation of metal SPR of ZnONPs (Gnanasangeetha and Thambavani, 2013; Nagarajan and Kuppusamy, 2013; Ali et al., 2016; Ashokan et al., 2017).

3.2. Morphology and crystallinity analyses

TEM data exhibit that the MFLE-ZnONPs were hexagonal and flower shaped nanostructures with significant monodispersity likely to be contributed by the soft cap of MFLE bio-actives (Fig. 1C). SEM analysis also validated the formation of flower shaped MFLE-ZnONPs formation (Fig. 1E). Structural and morphological behavior of ZnONPs are influenced by the functional groups *viz.* aromatic/aliphatic hydroxyl groups of MFLE bio-actives, which may interact with Zn^{2+} during nucleation, stabilization and subsequent decomposition of MFLE-Zn^{2+} complexes (Karnan and Selvakumar, 2016). Also, when hydroxyl group bridges formed among extract bio-actives, the bridg interacts with Zn^{2+} leading to flower-shaped morphologies of ZnO possibly by keeping the nascent complex in the proximity (Sharma, 2016). In the same line, *Azadirachta indica* extract, during nucleation and stabilization played a decisive role in configuring the various morphologies such as hexagonal disks, bullets, buds, cones, bundles and closed pine cone structured of ZnONPs (Madan et al., 2016). Furthermore, EDX based composition analysis of a selected field of SEM reveals that the MFLE-ZnONPs were composed of 78.47% zinc and 21.53% oxygen elements (Fig. 1F). The XRD pattern of MFLE-ZnONPs was shown in Fig. 1D. The XRD reflections obtained at 2θ degree corresponded to 100, 002, 101, 102, 110, 103, 200, 112, 201, 004 and 202 lattice plane with no extra peaks of impurities (Fig. 1D). All the diffraction peaks were indexed to hexagonal wurtzite type crystal symmetry of MFLE-ZnONPs (JCPDS Card No. 36-1451) with lattice constants a = 3.2498 Å, b = 3.2498 Å, and c = 5.2113 Å (PDF: 080-1268) (Ali et al., 2016; Velazquez et al., 2016). The average crystallite size of MFLE-ZnONPs was calculated by full-width-at-half-maximum (FWHM) of (101) Bragg reflection using Scherrer's formula (Tomalia et al., 1985), and was found to be 48.32 ± 2.5 nm.

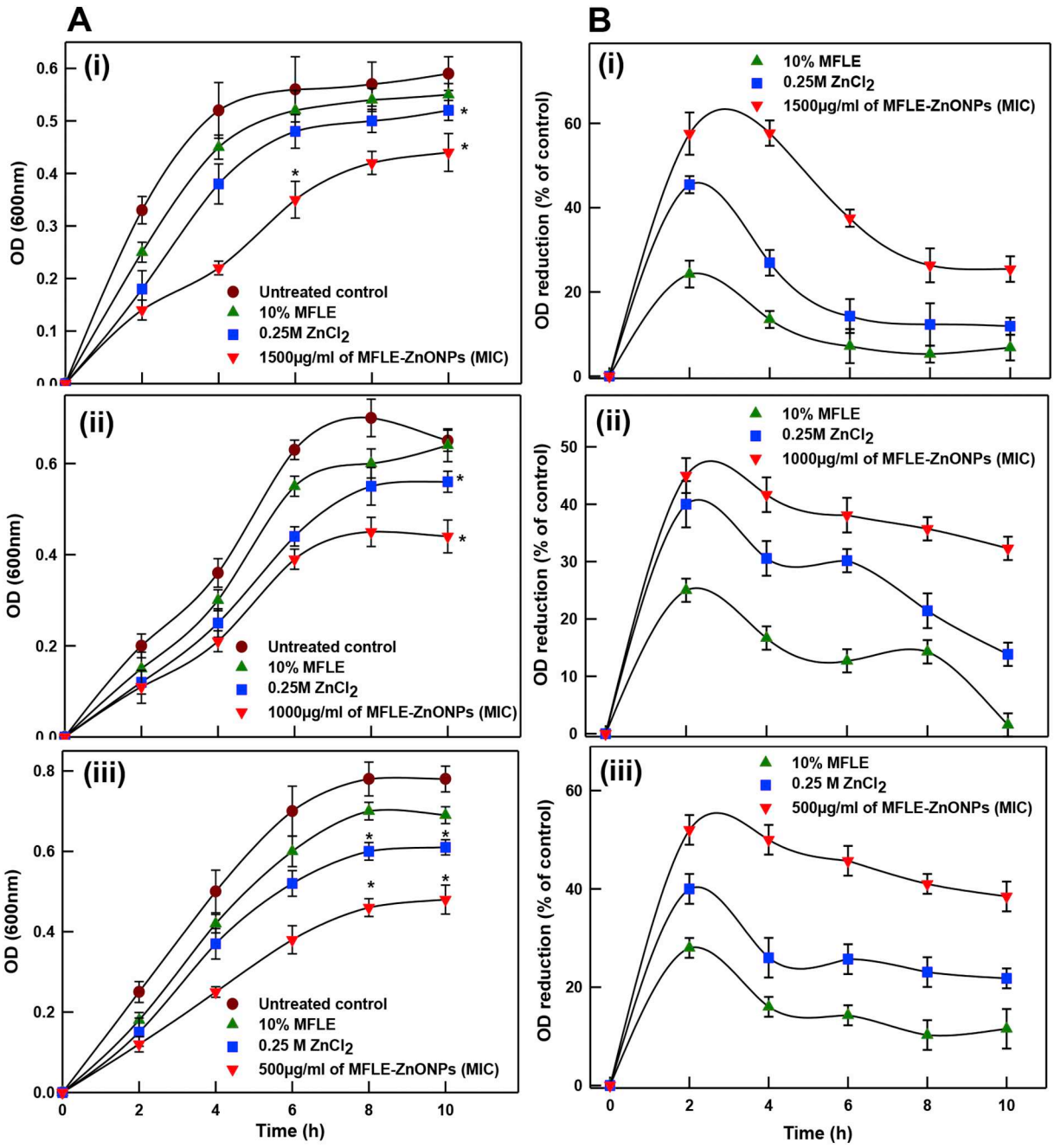

Fig. 5. Comparison of antibacterial activity of MFLE-ZnONPs with pristine MFLE and $ZnCl_2$ solutions against multi drug resistant (MDR) bacteria. (A) Changes in absorbance (600 nm) as an index of growth pattern of (i) *E. coli*-336, (ii) MRSA-1 and (iii) MSSA-2 at the MICs of MFLE-ZnONPs, MFLE and $ZnCl_2$. (B) Corresponding plots showing percent reduction in growth of (i) *E. coli*-336, (ii) MRSA-1 and (iii) MSSA-2.

3.3. FTIR and GC–MS analyses of MFLE-ZnONPs

FTIR stretching frequency and GC–MS spectra both infer the development of MFLE-ZnONPs. Fig. 3A showing a comparison among $ZnCl_2$ (spectrum-i), pristine MFLE (spectrum-ii) and the MFLE-ZnONPs (spectrum-iii) FTIR spectra revealing the surface adsorbed MFLE-bio-actives indicating their plausible role in bio-reduction of Zn^{2+} and stabilization of nascent ZnONPs. The vibration/stretching signatures at 3497 (–OH), 2926 (-NH), 2845 (> C-HO), 1637 (-C = O aromatic), 1045 and 723 (C-H in/out of plane bend) cm^{-1} reflect the involvement of 1°/2° amines (Chiguvare et al., 2016), amides-II (Vigneshwaran et al., 2007), aliphatic alkanes, aldehyde (Satapathy et al., 2017), amides (Sangeetha et al., 2011), carbonyl and amines (Kumari et al., 2015) in the reduction of Zn^{2+} to ZnONPs, respectively (Supplementary Table 1). Recently, Gupta et al. (2019) have also suggested that the capping can also be achieved due to > C = O, which acts as a linker *via* sharing O lone pair of an electron with electron deficient–OH capped nascent ZnONPs during nucleation phase. The appearance of a sharp band at 468 cm^{-1} is due to the bending vibrations of bond between host metal and oxygen components of MFLE-ZnONPs (Kwon et al., 2002; Emami-Karvani and Chehrazi, 2011; Ali et al., 2018).

On the other hand, GC–MS analysis of aqueous MFLE showed a total of 17 peaks (P) assigned to 15 types of MFLE bio-active compounds such as flavonoids (P1, P15, and P16), esters (P2, P5, P7, P8, P9, P10, P11, P12 and P13), and organic acids (P3, P4, P6, P14, and P17) (Fig. 3B, spectrum-i). Based on peak area percent, the most abundant MFLE bio-actives were P2- butyl 3-oxobut-2-yl ester ($C_{12}H_{18}O_5$; 13.53%), P6- cis-13-octadecenoic acid ($C_{18}H_{34}O_2$; 13.86%), P9- butyl

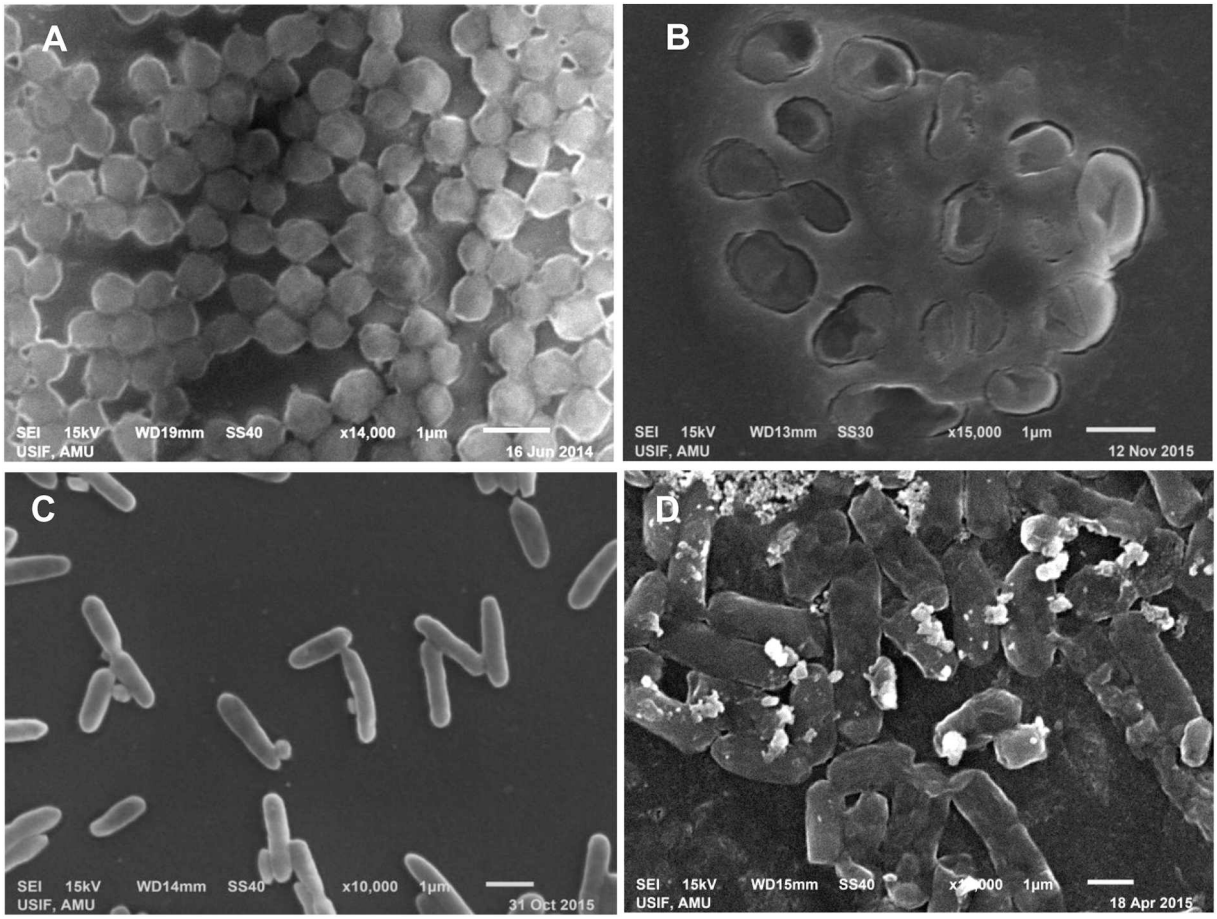

Fig. 6. Ultrastructural analysis of interaction between MFLE-ZnONPs and bacterial cells. Representative SEM images showing the cellular damage and surface binding of MFLE-ZnONPs with (B) methicillin resistant *S. aureus* and (D) *E. coli* cells (ESβL positive). The images in panels (A) and (C) show the untreated controls of *S. aureus* and *E. coli* cells, respectively.

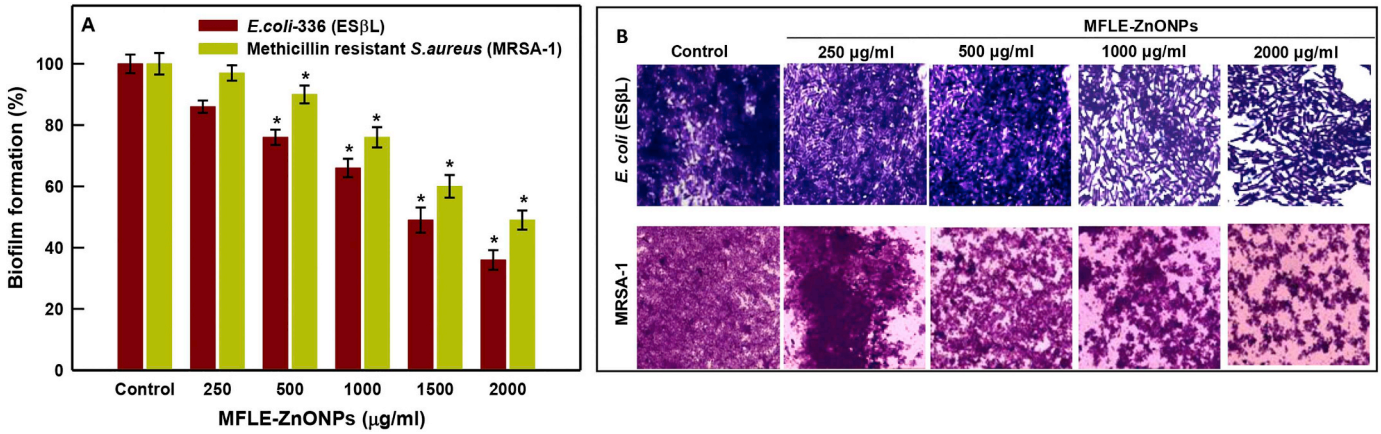

Fig. 7. Dose dependent biofilm reduction. (A) MFLE-ZnONPs concentration dependent inhibition of bacterial biofilm formation. The error bars represent mean ± SD of two independent experiments done in triplicate. $^{*}p < 0.05$ *vs* control. (B) Photomicrographs of biofilm formed by *E. coli*-336 (ESβL positive) and MRSA-1 grown in absence (control) and presence of MFLE-ZnONPs (250, 500, 1000 and, 2000 μg/ml).

linoleate ($C_{21}H_{40}O_4$; 10.71%), P13-α-monoolein ($C_{21}H_{40}O_4$; 16.05%), P16- dihydromyristicin ($C_{11}H_{14}O_3$; 6.12%) and, P17- desmethylnomifensine ($C_{15}H_{16}N_2$; 22.98%) and are speculated to play an active role in the bio-reduction of Zn^{2+} to ZnONPs during nucleation phase (Table 1). Furthermore, GC–MS analysis of MFLE-ZnONPs depicts the presence of butyl 3-oxobut-2-yl ester and α-monooleinester corona on the surface of MFLE-ZnONPs (Fig. 3B, spectrum-ii and Table 2), which unequivocally indicates that pi-conjugated core and delocalised malonate ester sites played a crucial role in binding ZnONPs *via* phobic, cation-pi, and steric interfaces (Gupta et al., 2019).

3.4. Antibacterial activities of MFLE-ZnONPs

3.4.1. Antibacterial activity, MIC and MBC determination of MFLE-ZnONPs

The antibacterial activity of MFLE-ZnONPs against *E. coli*-336 and MRSA-1 and MSSA-2 strains were primarily compared with MFLE alone

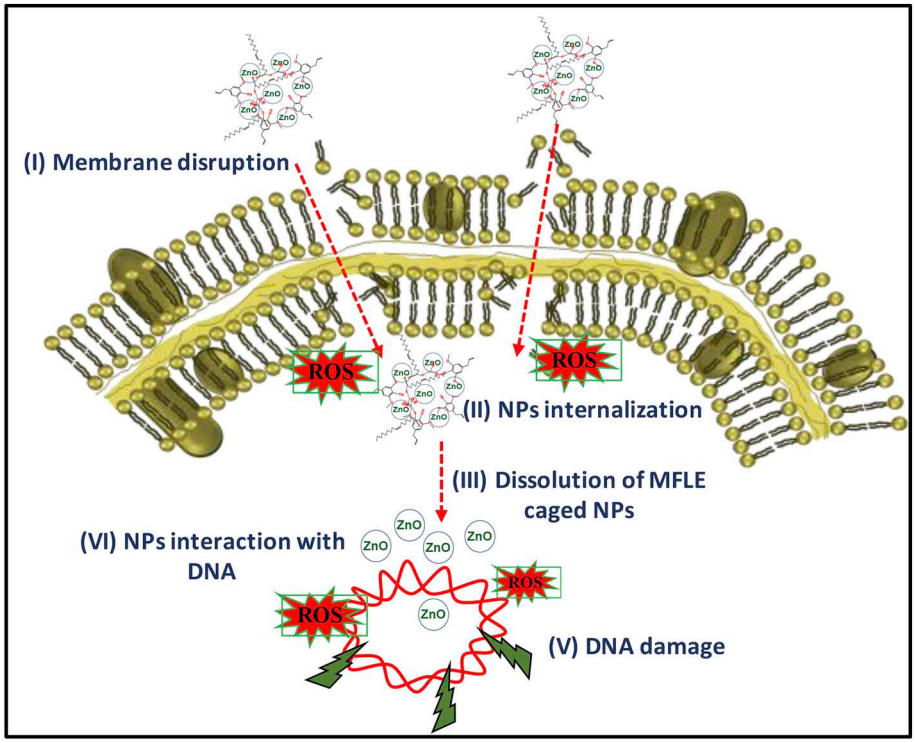

Fig. 8. Schematic presentation of plausible mechanism involved in MFLE-ZnONPs induced intracellular ROS and oxidative damage in bacteria.

by well diffusion assay. The data demonstrate a concentration dependent growth inhibition of clinical isolates by MFLE-ZnONPs treatment. Data presented in Fig. 4A reflects a dose dependent cytotoxic effect in the range of 500 to 2000 μg/ml of MFLE-ZnONPs demonstrating increase in zone of growth inhibition against *E. coli*-336 (17.0 ± 0.5 to 19.25 ± 1.0 mm), MSSA-2 (16.75 ± 0.8 to 19.0 ± 0.7 mm) and MRSA-1 (16.25 ± 1.0 to 18.25 ± 0.5 mm). The representative images of MFLE alone (100 μl) diluted to 1:100 (*v*/v) has produced non-cytotoxic effects on the tested strains (Fig. 4B ia, iia, iiia). Overall, MFLE-ZnONPs induced growth inhibition is in the order of *E. coli*-336 > *S. aureus* (MSSA-2) and *S. aureus* (MSSA-1). Besides the well diffusion based antibacterial screening, the MIC of MFLE-ZnONPs against *E. coli*-336, MRSA-1 and MSSA-2 were found to be 1500, 1000 and 500 μg/ml. Under identical conditions, the MBC were determined to be 2500, 2000 and 1500 μg/ml, respectively (Table 3). The MIC and MBC values obtained in our study indicate that Gram-positive MRSA-1 and MSSA-2 are more sensitive than Gram–negative *E. coli*-336. Our antibacterial data is supported well by the earlier finding indicating that the MIC and MBC values of commercial ZnONPs (20–80 nm) against *E. coli* is 1250 and 2500 μg/ml and, 312 and 1250 μg/ml against *S. aureus*, respectively (Yu et al., 2014). A valid reason for the differences in susceptibility of tested clinical isolates is the hyper susceptibility of Gram-positive *S. aureus* cells, as compared to Gram–negative *E. coli,* which could be assigned to the differences in cell wall structure, cell physiology, metabolism or degree of contact (Li et al., 2004). Besides, ZnONPs are well known to augment bacterial activities by several possible mechanisms. Reactive oxygen species (ROS) generation trigerred by ZnONPs promptly reduce the growth of Gram-positive *S. aureus* and Gram–negative *E. coli* by accumulation or deposition on the cell surface (Ali et al., 2016). ZnONPs bind to the surface of bacteria through electrostatic forces (Jones et al., 2008) and subsequently releaese zinc ions on the membranes distorting the cell wall which ultimately results in the leakage of intracellular components and cell death (Jayaseelan et al., 2012).

3.4.2. Planktonic growth inhibition analysis

Based on the MIC of MFLE-ZnONPs against *E. coli*-336, MSSA-2 and MRSA-1 strains, a time and dose dependent reduction in cell proliferation was recorded (Fig. 5A i-iii). Relative to control, after 10 h of incubation with MFLE-ZnONPs (MIC 1500 μg/ml), MFLE alone (10%) and $ZnCl_2$ (0.25 M) *E. coli*-336 survival dropped to 25%, 11.8% and 6.7% (Fig. 5Bi), respectively. The growth dynamics of MRSA-1 showed survival reduction of 32.3%, 13.8%, and 1.5% with MFLE-ZnONPs (MIC 1000 μg/ml), MFLE alone (10%) and $ZnCl_2$ (0.25 M) (Fig. 5Bii). Similarly, MSSA-2 growth reduced to 38.46%, 21.7% and 11.5% with MFLE-ZnONPs (MIC 500 μg/ml), MFLE alone (10%) and $ZnCl_2$ (0.25 M) (Fig. 5Biii). Similarly, Azizi et al. (2016) have shown that the *Anchusa italica* extract capped-ZnONPs (14 nm) are more effective against Gram-positive than Gram-negative bacteria. In the same line, Emami-Karvani and Chehrazi (2011) have also shown that the MIC value of chemically prepared ZnONPs for *E. coli* and *S. aureus* are 1000 and 500 μg/ml, respectively. However, compared to antibacterial activities of *Aristolochia indica* capped-ZnONPs (22.5 nm), MFLE-ZnONPs showed significantly lower toxicity against Gram-positive and Gram-negative bacteria (Steffy et al., 2018). Also, the representative SEM images in Fig. 6A-D clearly show the interaction of MFLE-ZnONPs (at MICs values) with *S. aureus* and *E. coli* cells revealing NPs induced cellular damage *via* loss of native rod and coccoid shapes due to the formation of pits and cavities in the treated bacterial cells. The SEM analysis aptly supports the hyper susceptibility of Gram-positive *S. aureus* than Gram-negative *E. coli* cells. Overall, the loss of native shapes and integration of cell wall affirmed the cellular internalization of ZnONPs observed earlier in *E. coli* and *S. aureus* bacteria (Brayner et al., 2006; Ali et al., 2016).

3.4.3. Inhibition of biofilm by MFLE-ZnONPs

MFLE-ZnONPs were further evaluated for anti-biofilm activity. *E. coli*-336 when cultured with MFLE-ZnONPs (250, 500, 1000, 1500 and 2000 μg/ml) for 24 h showed 14%, 24%, 34%, 51% and 64% sharp decline in biofilm formation. Under identical conditions, MRSA-1 cultured with MFLE-ZnONPs (250, 500, 1000, 1500 and 2000 μg/ml) for 24 h showed 3%, 10%, 24%, 40% and 51% reduction in biofilm formation (Fig. 7A). The representative micrographs obtained after MFLE-ZnONPs exposure explicitly show the concentration-dependent depletion in biofilm formation by *E. coli* and *S. aureus* cells (Fig. 7B). Similar dose-dependent patterns in biofilm formation have been observed against Gram-negative *E. coli* and *P. aeruginosa,* and Gram-positive *S.*

aureus cells in our earlier studies demonstrating the antibiofilm efficacy of bio-inspired Ag, ZnO, CuO and α-Fe_2O_3NPs (Ali et al., 2015, 2016, 2018, 2019). *E. coli* and *S. aureus* both are known to produce potent extracellular matrix/biofilm consisting of extracellular polysaccharide, proteins and nucleic acids *etc.* (Ali et al., 2018). Despite adequate chemotherapeutics formulations/antibiotic therapies, microbial biofilms allow colony survival and dispersal (Costerton et al., 1999; Hall-Stoodley et al., 2004; Fux et al., 2005). Such constrains prompt clinicians to seek alternatives to manage the aggregation of biofilms clinically. Combating MDR bacterial isolates *via* the novel approach of nanomaterials treatment demonstrated significant reduction in biofilm formation (Wahab et al., 2013; Dwivedi et al., 2014; Wahab et al., 2016; Khan et al., 2015). In addition, the bio-inspired NPs fabricated by use of different medicinal plant extracts have also produced significantly greater antibacterial effects *in vitro* quorum quenching trials, as compared to their bare surface micro and nano-sized inorganic analogues and pure extracts. Similarly, our anti-biofilm data reflected an extraordinary propensity of penetration ability into the bacterial cells *via* highly organized biofilm matrices. In the same line, we have recently demonstrated that compared to comercially procured bare surface nano scale analogues, our ALE-α-Fe_2O_3NPs and *Eucallyptus globulus* extract (ELE) capped-CuONPs possess significantly higher propensity of internalization and surface contact within biofilm matrices (Ali et al., 2018, 2019). Consequently, as illustrated schematically in Fig. 8 the internalization of MFLE-ZnONPs can be speculated to trigger the intracellular reactive oxygen species generation and ultimately cause cell death by augmenting oxidative stress (Ali et al., 2016, 2018, 2019; Ahmed et al., 2018).

4. Conclusions

We demonstrate a comprehensive role of *M. fragrans* bio-actives in the mechanics of bio-synthesis of ZnONPs. GC–MS analyses affirmed that the MFLE bio-actives played a significant role as bio-reluctance in converting Zn^{2+} precursors to MFLE-ZnONPs during nucleation phase. Whereas, the MFLE esters, butyl 3-oxobut-2-yl ester ($C_{12}H_{18}O_5$) and α-monoolein ($C_{21}H_{40}O_4$) were also involved as surface capping/stabilizing agents. FTIR further validated the role of MFLE bio-actives in bio-synthesis of NPs. Ultrastructural analysis of reduced NPs revelaed flower-like shapes of MFLE-ZnONPs, whereas XRD results confirmed pure crystalline phase of a size 48.32 ± 2.5 nm. Overall our data provide a novel one-step/one-pot approach for the bio-synthesis of MFLE-ZnONPs using MFLE bio-actives as reducing, stabilizing and capping agent. MFLE-ZnONPs exhibited superior antibacterial and antibiofilm activities against MDR Gram-negative and Gram-positive bacteria. Consequently, MFLE-ZnONPs may be an unprecedented alternative against prominent biofilm infections in the biomedical settings.

Declaration of Competing Interest

There is no conflict of interest.

Acknowledgments

The authors extend their appreciation to the International Scientific Partnership Program ISPP at King Saud University for funding this research work through ISPP# 0031.

Appendix A. Supplementary data

Supplementary data to this article can be found online at https://doi.org/10.1016/j.mimet.2019.105716.

References

Ahmed, B., Hashmi, A., Khan, M.S., Musarrat, J., 2018. ROS mediated destruction of cell membrane, growth and biofilms of human bacterial pathogens by stable metallic AgNPs functionalized from bell pepper extract and quercetin. Adv. Pow. Technol. 29, 1601–1616.

Ali, K., Ahmed, B., Dwivedi, S., Saquib, Q., Al-Khedhairy, A.A., Musarrat, J., 2015. Microwave accelerated green synthesis of stable silver nanoparticles with *Eucalyptus globulus* leaf extract and their antibacterial and antibiofilm activity on clinical isolates. PLoS One 1, e0131178.

Ali, K., Dwivedi, S., Azam, A., Saquib, Q., Al-Said, M.S., Alkhedhairy, A.A., Musarrat, J., 2016. *Aloe vera* extract functionalized zinc oxide nanoparticles as nanoantibiotics against multi-drug resistant clinical bacterial isolates. J. Coll. Interf. Sci. 472, 145–156.

Ali, K., Ahmed, B., Khan, M.S., Musarrat, J., 2018. Differential surface contact killing of pristine and low EPS *Pseudomonas aeruginosa* with *Aloe vera* capped hematite (α-Fe_2O_3) nanoparticles. J. Photochem. Photobiol. B Biol. 188, 146–158.

Ali, K., Ahmed, B., Ansari, S.M., Saquib, Q., Al-Khedhairy, A.A., Dwivedi, S., Alshaeri, M., Khan, M.S., Musarrat, J., 2019. Comparative *in situ* ROS mediated killing of bacteria with bulk analogue, Eucalyptus leaf extract (ELE)-capped and bare surface copper oxide nanoparticles. Mater. Sci. Eng. C. 100, 747–758.

Al-Sheddi, E.S., Farshori, N.N., Al-Oqail, M.M., Al-Massarani, S.M., Saquib, Q., Wahab, R., Musarrat, J., Al-Khedhairy, A.A., Siddiqui, M.A., 2018. Anticancer potential of green synthesized silver nanoparticles using extract of *Nepeta deflersiana* against human cervical cancer cells (HeLA). Bioinorg. Chem. App. 2018, 9390784.

Aoki, T., Hatanaka, Y., 2000. ZnO diode fabricated by excimer-laser doping. Appl. Phys. Lett. 76, 3257–3258.

Ashokan, A.P., Paulpandi, M., Dinesh, D., Murugan, K., Vadivalagan, C., Benelli, G., 2017. Toxicity on dengue mosquito vectors through *Myristica fragrans*-synthesized zinc oxide nanorods, and their cytotoxic effects on liver cancer cells (HepG2). J. Clust. Sci. 28, 205–226.

Azizi, S., Mohamad, R., Bahadoran, A., Bayat, S., Rahim, R.A., Ariff, A., Saad, W.Z., 2016. Effect of annealing temperature on antimicrobial and structural properties of bio-synthesized zinc oxide nanoparticles using flower extract of *Anchusa italica*. J. Photochem. Photobiol. Biol. 161, 441–449.

Balakrishnan, S., Sivaji, I., Kandasamy, S., Duraisamy, S., Kumar, N.S., Gurusubramanian, G., 2017. Biosynthesis of silver nanoparticles using *Myristica fragrans* seed (nutmeg) extract and its antibacterial activity against multidrug-resistant (MDR) *Salmonella enterica* serovar *Typhi* isolates. Env. Sci. Poll. Res. 24, 14758–14769.

Bhosale, A.M., Bhanage, M.B., 2015. Silver nanoparticles: synthesis, characterization and their application as a sustainable catalyst for organic transformations. Curr. Org. Chem. 19, 708–727.

Brayner, R., Ferrari-Illiou, R., Briviois, N., Djediat, S., Benedetti, M.F., Fievet, F., 2006. Toxicological impact studies based on *Escherichia coli* bacteria in ultrafine ZnO nanoparticles colloidal medium. Nano Lett. 6, 866–870.

Chiguvare, H., Oyedeji, O.O., Matewu, R., Aremu, O., Oyemitan, I.A., Oyedeji, A.O., Nkeh-Chungag, B.N., Songca, S.P., Mohan, S., Oluwafemi, O.S., 2016. Synthesis of silver nanoparticles using buchu plant extracts and their analgesic properties. Mol. 21, 774–777.

Costerton, J.W., Stewart, P.S., Greenberg, E.P., 1999. Bacterial biofilms: a common cause of persistent infections. Sci. 284, 1318–1322.

Das, A., Wang, D.Y., Leuteritz, A., Subramaniam, K., Greenwell, H.C., Wagenknecht, U., Heinrich, G., 2011. Preparation of zinc oxide free, transparent rubber nanocomposites using a layered double hydroxide filler. J. Mater. Chem. 21, 719–7200.

Dwivedi, S., Wahab, R., Khan, F., Mishra, Y.K., Musarrat, J., Al-Khedhairy, A.A., 2014. Reactive oxygen species mediated bacterial biofilm inhibition via zinc oxide nanoparticles and their statistical determination. PLoS One 9, e111289.

Emami-Karvani, Z., Chehrazi, P., 2011. Antibacterial activity of ZnO nanoparticle on gram-positive and gram-negative bacteria. Afr. J. Microbiol. Res. 5, 1368–1373.

Fux, C.A., Costerton, J.W., Stewart, P.S., Stoodley, P., 2005. Survival strategies of infectious biofilms. Trends Microbiol. 13, 34–40.

Gnanasangeetha, D., Thambavani, S., 2013. One pot synthesis of zinc oxide nanoparticles via chemical and green method. Res. J. Mater. Sci. 1, 1–8.

Gupta, A.D., Bansal, V.K., Babu, V., Maithil, N., 2013. Chemistry, antioxidant and antimicrobial potential of nutmeg (*Myristica fragrans* Houtt). J. Genetic Eng. Biotech. 11, 25–31.

Gupta, R., Das, N., Singh, M., 2019. Fabrication and surface characterisation of c-ZnO loaded TTDMM dendrimer nanocomposites for biological applications. Appl. Surf. Sci. 484, 781–796.

Hall-Stoodley, L., Costerton, J.W., Stoodley, P., 2004. Bacterial biofilms: from the natural environment to infectious diseases. Nat. Rev. Microbiol. 2, 95–108.

Hameed, A.S.H., Karthikeyan, C., Ahamed, A.P., Thajuddin, N., Alharbi, N.S., Alharbi, S.A., Ravi, G., 2016. In-vitro antibacterial activity of ZnO and Nd doped ZnO nanoparticles against ESBL producing *Escherichia coli* and *Klebsiella pneumonia*. Sci. Rep. 6, 1–11.

Helen, P.A.M., Vargheese, T.A., Jeeja Kumari, J.J., Abiramy, M.R., Sajina, N., Jaya Sree, S., 2012. Phytochemical analysis and anticancer activity of essential oil from *Myristica fragrans*. Int. J. Curr. Pharma. Rev. Res. 2, 188–198.

Jayaseelan, C., Rahuman, A.A., Kirthi, A.V., Marimuthu, S., Santhoshkumar, T., Bagavan, A., Gaurav, K., Karthik, L., Rao, K.B., 2012. Novel microbial route to synthesize ZnO nanoparticles using Aeromonas hydrophila and their activity against pathogenic bacteria and fungi. Spect. Acta Part A: Mol. Biomol. Spect. 90, 78–84.

Jones, N., Ray, B., Ranjit, K.T., Manna, A.C., 2008. Antibacterial activity of ZnO nanoparticle suspensions on a broad spectrum of microorganisms. FEMS Microbiol. Lett. 279, 71–76.

Karnan, T., Selvakumar, S.A., 2016. Biosynthesis of ZnO nanoparticles using rambutan *Nephelium lappaceum* (L) peel extract and their photocatalytic activity on methyl orange dye. J. Mol. Struc. 1125, 358–365.
Khan, S.T., Al-Khedhairy, A.A., Musarrat, J., 2015. ZnO and TiO_2 nanoparticles as novel antimicrobial agents for oral hygiene: a review. J. Nano. Res. 17, 276.
Kumari, M.M., Jacob, J., Philip, D., 2015. Green synthesis and applications of Au–Ag bimetallic nanoparticles. Spectrochim. Acta Mol. Biomol. Spectrosc. 137, 185–192.
Kwon, Y.J., Kim, K.H., Lim, C.S., Shim, K.B., 2002. Characterization of ZnO nanopowders synthesized by the polymerized complex method via an organo chemical route. J. Ceram. Proc. Res. 3, 146–149.
Li, H., Wang, J., Liu, H., Yang, C., Xu, H., Li, X., Cui, H., 2004. Sol–gel preparation of transparent zinc oxide films with highly preferential crystal orientation. Vac. 77, 57–62.
Lima, R.K., Cardoso, M. das G., Andrade, M.A., Guimarães, P.L., Batista, L.R., Nelson, D.L., 2012. Bactericidal and antioxidant activity of essential oils from *Myristica fragrans* Houtt and *Salvia microphylla* H.B.K. J. Am. Oil Chem. Soc. 89, 523–528.
Look, D.C., Reynolds, D.C., Sizelove, J.R., Jones, R.L., Litton, C.W., Cantwell, G., Harsch, W.C., 1998. Electrical properties of bulk ZnO. Sol. St. Comm. 105, 399–401.
Madan, H.R., Sharma, S.C., Suresh, D., Vidya, Y.S., Nagabhushana, H., Rajanaik, H., Anantharaju, K.S., Prashantha, S.C., Maiya, P.S., 2016. Facile green fabrication of nanostructure ZnO plates, bullets, flower, prismatic tip, closed pine cone: their antibacterial, antioxidant, photoluminescent and photocatalytic properties. Spectro. Acta Part A 152, 404–416.
Musarrat, J., Ali, K., Ansari, M.A., Saquib, Q., Siddiqui, M., Khan, S.T., Alkhedhairy, A.A., 2015. Green synthesis of nanoparticles and their role as nano-antibiotics and anti-biofilm agents. Planta Med. 81, OA44.
Nagarajan, S., Kuppusamy, K.A., 2013. Extracellular synthesis of zinc oxide nanoparticles using seaweeds of Gulf of Mannar, India. J. Nanobiotechnol. 11, 39.
Nasajpour, A., Mandla, S., Shree, S., Mostafavi, E., Sharifi, R., Khalilpour, A., Saghazadeh, S., Hassan, S., Mitchell, M.J., Leijten, J., Hou, X., 2017. Nanostructured fibrous membranes with rose spike-like architecture. Nano Lett. 17, 6235–6240.
Nasajpour, A., Ansari, S., Rinoldi, C., Rad, A.S., Aghaloo, T., Shin, S.R., Mishra, Y.K., Adelung, R., Swieszkowski, W., Annabi, N., Khademhosseini, A., 2018. A multifunctional polymeric periodontal membrane with osteogenic and antibacterial characteristics. Adv. Funct. Mater. 28, 1703437.
Pearton, S.J., Norton, D.P., Ip, K., Heo, Y.W., 2004. Recent advances in processing of ZnO. J. Vac. Sci. Tech. B 22, 932–948.
Sangani, M.H., Moghaddam, M.N., Forghanifard, M.M., 2015. Inhibitory effect of zinc oxide nanoparticles on *Pseudomonas aeruginosa* biofilm formation. Nanomed. J. 2, 121–128.
Sangeetha, G., Rajeshwari, S., Venckatesh, R., 2011. Green synthesis of zinc oxide nanoparticles by *Aloe barbadensis* miller leaf extract: structure and optical properties. Mater. Res. Bull. 46, 2560–2566.
Satapathy, S., Paikaray, S., Thirunavoukkarasu, M., Panda, C.R., Subbudhi, E., 2017. Biosynthesis and characterization of silver nanoparticles derived from marine bivalve *Donax cuneatus* (Linnaeus) and assessment of its antimicrobial potential. Inorg. Nano-Met. Chem. 47, 1044–1048.
Shahbazali, E., Hessel, V., Noel, T., Wang, Q., 2014. Metallic nanoparticles made in flow and their catalytic applications in organic synthesis. Nanotechnol. Rev. 3, 65–86.
Sharma, S.C., 2016. ZnO nano-flowers from *Carica papaya* milk: degradation of Alizarin Red-S dye and antibacterial activity against *Pseudomonas aeruginosa* and *Staphylococcus aureus*. Optik 127, 6498–6512.
Sharma, G., Sharma, A.R., Kurian, M., Bhavesh, R., Nam, J.S., Lee, S.S., 2014. Green synthesis of silver nanoparticle using *Myristica fragrans* (Nutmeg) seed extract and its biological activity. Dig. J. Nanomat. Biostruct. 9.
Steffy, K., Shanthi, G., Maroky, A.S., Selvakumar, S., 2018. Enhanced antibacterial effects of green synthesized ZnO NPs using Aristolochia indica against multi-drug resistant bacterial pathogens from diabetic foot ulcer. J. Infec. Pub. Health 11, 463–471.
Sutradhar, P., Saha, M., 2015. Synthesis of zinc oxide nanoparticles using tea leaf extract and its application for solar cell. Bull. Mat. Sci. 38, 653–657.
Tang, Z.K., Wong, G.K.L., Yu, P., 1998. Room-temperature ultraviolet laser emission from self-assembled ZnO microcrystallite thin films. Appl. Phys. Lett. 72, 3270.
Tomalia, D.A., Baker, H., Dewald, J., Hall, M., Kallos, G., Martin, S., Ryder, J., Smith, P., 1985. A new class of polymers: starburst-dendritic macromolecules. Poly. J. 17.
Velazquez, N.G.A., Vargas-García, J.R., Aguilar-Hernández, J., Vega-Becerra, O.E., Chen, F., Shen, Q., Zhang, L., 2016. Optical and electrical properties of (002)-oriented ZnO films prepared on amorphous substrates by sol-gel spin-coating. Mater. Res. 19, 113–117.
Vigneshwaran, N., Kathe, A.A., Varadarajan, P.V., Nachane, R.P., Balasubramanya, R.H., 2007. Biomimetics of silver nanoparticles by white rot fungus, *Phaenerochaete chrysosporium*. Coll. Surf. B. Biointerf. 53, 55–59.
Vilas, V., Philip, D., Mathew, J., 2014. Catalytically and biologically active silver nanoparticles synthesized using essential oil. Spectro. Acta Part A 11, 743–750.
Wahab, R., Khan, S.T., Dwivedi, S., Ahamed, M., Musarrat, J., Al-Khedhairy, A.A., 2013. Effective inhibition of bacterial respiration and growth by CuO microspheres composed of thin nanosheets. Coll. Surf. B. Biointerf. 111, 211–217.
Wahab, R., Khan, F., Mishra, Y.K., Musarrat, J., Al-Khedhairy, A.A., 2016. Antibacterial studies and statistical design set data of quasi zinc oxide nanostructures. RSC Adv. 6, 32328–32339.
Yu, J., Zhang, W., Li, Y., Wang, G., Yang, L., Jin, J., Chen, Q., Huang, M., 2014. Synthesis, characterization, antimicrobial activity and mechanism of a novel hydroxyapatite whisker/nano zinc oxide biomaterial. Biomed. Mat. 10, 015001.